Published online 24 July 2021

Nucleic Acids Research, 2021, Vol. 49, No. 14 **8199–8213**
https://doi.org/10.1093/nar/gkab634

Motif WFYY of human PrimPol is crucial to stabilize the incoming 3′-nucleotide during replication fork restart

Patricia A. Calvo[1], María I. Martínez-Jiménez[1], Marcos Díaz[2], Gorazd Stojkovic[3], Kazutoshi Kasho[3,4], Susana Guerra[1], Sjoerd Wanrooij[3,*], Juan Méndez[2,*] and Luis Blanco[1,*]

[1]Centro de Biología Molecular Severo Ochoa, CSIC-UAM, 28049, Madrid, Spain, [2]Spanish National Cancer Research Centre (CNIO), 28029, Madrid, Spain, [3]Department of Medical Biochemistry and Biophysics, Umeå University, Umeå, Sweden and [4]Department of Molecular Biology, Graduate School of Pharmaceutical Sciences, Kyushu University, Fukuoka 812-8582, Japan

Received February 05, 2021; Revised July 06, 2021; Editorial Decision July 08, 2021; Accepted July 12, 2021

ABSTRACT

PrimPol is the second primase in human cells, the first with the ability to start DNA chains with dNTPs. PrimPol contributes to DNA damage tolerance by restarting DNA synthesis beyond stalling lesions, acting as a TLS primase. Multiple alignment of eukaryotic PrimPols allowed us to identify a highly conserved motif, WxxY near the invariant motif A, which contains two active site metal ligands in all members of the archeo-eukaryotic primase (AEP) superfamily. *In vivo* and *in vitro* analysis of single variants of the WFYY motif of human PrimPol demonstrated that the invariant Trp^{87} and Tyr^{90} residues are essential for both primase and polymerase activities, mainly due to their crucial role in binding incoming nucleotides. Accordingly, the human variant F88L, altering the WFYY motif, displayed reduced binding of incoming nucleotides, affecting its primase/polymerase activities especially during TLS reactions on UV-damaged DNA. Conversely, the Y89D mutation initially associated with High Myopia did not affect the ability to rescue stalled replication forks in human cells. Collectively, our data suggest that the WFYY motif has a fundamental role in stabilizing the incoming 3′-nucleotide, an essential requisite for both its primase and TLS abilities during replication fork restart.

INTRODUCTION

The DNA replication machinery is responsible for the integrity and stability of genetic information, making use of several DNA polymerases to replicate the genome, but also to repair and tolerate lesions. Replicases are assisted by specialized enzymes called primases, which make short RNA strands serving as 'primers' (1). Human cells have two DNA primases: Prim1 that operates at nuclear DNA and is a heterodimer (p48 + p58) wherein p48 is the catalytic subunit. A complex of this primase with Polα is responsible for initiating synthesis of the leading strand at each origin, and for recurrent priming of Okazaki fragments at the lagging strand during DNA replication (2).

The second human primase is PrimPol, an enzyme with combined DNA primase and TLS polymerase activities that is involved in nuclear and mitochondrial replication. Cells lacking PrimPol are viable, but fail to maintain normal nuclear fork progression rate even in the absence of DNA damage (3) and display impaired mitochondrial DNA replication (4,5). PrimPols have been described in plasmids (6), bacteria (7), archea (8) and eukaryotes (4). While PrimPols belong to the same Archeal-Eukaryotic Primase (AEP) super-family as conventional primases, they combine both DNA primase and DNA polymerase activities in a single polypeptide and a single active site (4,9). Human PrimPol contains the active-site motifs A, B and C, shared by members of the AEP superfamily, and a specific Zn-finger domain similar to that of herpesvirus UL52 primase (10), which specifically interacts with the initiating 5′ nucleotide (11,12). *In vivo* studies demonstrated that PrimPol assists DNA replication by repriming stalled forks ahead of lesions or obstacles, leaving behind an unreplicated gap to be repaired post-replicatively (3,13,14). This repriming activity also facilitates replication traverse of DNA interstrand crosslinks (15). In addition, PrimPol efficiently bypasses certain DNA lesions such as 8-oxo-7,8-

*To whom correspondence should be addressed. Tel: +34 911964685; Fax: +34 911964401; Email: lblanco@cbm.csic.es
Correspondence may also be addressed to Juan Méndez. Tel: +34 917328000; Fax: +34 917328033; Email: jmendez@cnio.es
Correspondence may also be addressed to Sjoerd Wanrooij. Tel: +46 722460309; Email: sjoerd.wanrooij@umu.se

dihydrodeoxyguanosine (8-oxo-dG) by directly incorporating either dNTPs or NTPs opposite the lesion (4,16–18). DNA lesions like pyrimidine dimers (6-4PP, CPD) or AP sites can also be bypassed by PrimPol by reannealing the primer ahead of the lesion (16). The *in vivo* relevance of this TLS potential is currently unknown.

In this study, we identified the conserved motif WxxY at the N-terminus of eukaryotic PrimPols, in proximity to the active site motif A conserved in the whole AEP superfamily. The flanking amino acids of this motif (Trp^{87} and Tyr^{90} in human PrimPol) are the most invariant in animal and plant PrimPols. By site-directed mutagenesis and a combination of *in vitro* and *in vivo* analysis, we show that these two invariant residues are irrelevant for ssDNA binding, but essential to form the pre-ternary complex PrimPol:ssDNA:dNTP (11), an intermediate which precedes the primase action required to rescue stalled replication forks. By extrapolation to the 3D-structure of human PrimPol in complex with DNA and deoxynucleotide (19), which reflects its polymerase mode, we propose that the WxxY motif plays an indirect role in stabilizing the 3′-incoming nucleotide in both TLS primase and polymerase activities. Accordingly, both activities were lost when Trp^{87} and Tyr^{90} were mutated to glycine and aspartate, respectively. Interestingly, a non-conservative mutation at Phe^{88} (F88L) showed a marked reduction in the affinity for the incoming 3′-nucleotide that preferentially affected the primase and TLS reactions on UV-damaged DNA. Conversely, the Y89D variant, which was previously claimed to be associated with High Myopia (20,21), and more recently with Progressive External Ophtalmoplegia (PEO; 22), had only a minor effect on the PrimPol catalytic activities. Our data is therefore consistent with extensive genetic analysis that indicated that Y89D PrimPol variant occurs randomly in the population and is not overrepresented in patients with High Myopia (23).

MATERIALS AND METHODS

Oligonucleotides, nucleotides and enzymes

Conventional DNA oligonucleotides were synthesized by Sigma Aldrich (St Louis, MO, USA). Oligonucleotides used in the *in vitro* DNA polymerization assays were purified by 8 M urea-20% polyacrylamide gel electrophoresis and 5′-labeled with [γ-^{32}P]*ATP* (3000Ci/ mmol) from Perkin-Elmer (Waltham, MA, USA) and T4 polynucleotide kinase (New England Biolabs, Ipswich, MA, USA) for 45 min at 37°C. Hybridizations were performed in 50 mM Tris–HCl pH 7.5 and 0.3 M NaCl for 10 min at 80°C and cooled down to room temperature. Unlabeled ultrapure dNTPs were supplied by GE Healthcare (Chicago, IL, USA). [γ-^{32}P]ATP, [α-^{32}P]dGTP and [α-^{32}P]dTTP were obtained from Perkin Elmer. Human Polγ holoenzyme (subunits A + B) was kindly provided by M. Falkenberg's lab (Gothenburg University, Sweden). Human full length PolDIP2 (amino acid 1-368, c-terminally His6 tagged) was cloned into pET21d plasmid, introduced into *E. coli* ArcticExpress (DE3) cells, and purified by Ni-NTA beads and HiTrap Heparin column (GE Healthcare).

Construction of PrimPol mutants

For *in vitro* analysis, desired point mutations were introduced in the expression plasmid pET16::PrimPol following the 'quick-change' site-directed mutagenesis protocol from Stratagene. Human wild-type (WT) PrimPol and the mutated variants (W87G, F88L, Y89D, Y90D) were expressed in *Escherichia coli* BL21 (DE3) pRIL and purified as previously described (4). To further support the data, the Y89D mutant was expressed and purified by following a different procedure, as previously described (24). For *in vivo* analysis, DNA sequences encoding WT PrimPol, or PrimPol variants AxA (3), W87G, F88L, Y89D and Y90D were cloned into Gateway expression vectors introducing an N-terminal V5 tag (Invitrogen, Carlsbad, CA, USA). Transient transfections were performed using Lipofectamine 2000 (Invitrogen).

Primary sequence alignment and 3D-visualization

Multiple alignments of the indicated amino acid sequence were performed using the MULTALIN server (25; http://multalin.toulouse.inra.fr/multalin/). Three-dimensional images were created with Swiss-PdbViewer (DeepView) program, developed within the Swish Institute of Bioinformatics (SIB) at the Structural Bioinformatics Group at the Biozentrum in Basel, and using human PrimPol PDB ID: 5L2X, which corresponds to the crystal structure of human PrimPol ternary complex (19).

DNA primase assays

DNA primase activity of PrimPol WT and the mutants of the WFYY motif were evaluated using a 29-mer oligonucleotide (3′-T_{15}GTCCT_{10}-5′) as template, which contains a putative herpesvirus priming initiation site (GTCC) (4,26). The reaction mixture (20 μl) contained buffer R (50 mM Tris pH 7.5, 5% Gly, 75 mM NaCl, 1 mM $MnCl_2$, 1 mM DTT and 0.1 μg/μl BSA), PrimPol WT or mutated variants of WFYY (200 nM), [γ-^{32}P]ATP (16 nM; 3000 Ci/mmol) and increasing concentrations of dGTP (1, 10 and 100 μM). The reaction was incubated during 30 min at 30°C. Reactions were stopped by addition of formamide loading buffer (10 mM EDTA, 95% v/v formamide and 0.3% w/v xylenecyanol) and loaded in 8 M urea-containing 20% polyacrylamide sequencing gels. Radiolabeled bands corresponding to nascent primers were detected by autoradiography, and used to quantify the primase activity by densitometry of the autoradiographs. Quantitation of the primase activity**.** When indicated, an oligonucleotide with the GTCA core sequence (3′-T_{15}GTCAT_{10}-5′) was used as a template in the presence of [α-^{32}P]dGTP (16 nM; 3,000 Ci/mmol) and ATP (100 μM), or ATP + dTTP (100 μM), as indicated. The reaction mixture (20 μl) contained buffer R and PrimPol WT or mutated variants (200 nM) were incubated during 30 min at 30°C. Reactions were stopped and analyzed as described above.

To measure processivity during primase synthesis, a different template was used (3′T_{29}**GTC**AGACAGCAT_{20} 5′), in the presence of [γ-^{32}P]ATP (16 nM; 3,000 Ci/mmol), dGTP + dCTP + dTTP (100 μM each), WT PrimPol or mutants F88L and Y89D (at various concentrations; 100

to 400 nM), and the incubation was carried out for various times (5, 20, 40 and 60 min) at 30°C.

The primase capacity of the WFYY mutants (100 nM) was evaluated in combination with the mitochondrial DNA polymerase gamma (Polγ; 20 nM), using M13 ssDNA (5 ng/μl) as template. Incubations were performed in reaction buffer (50 mM Tris–HCl pH 7.5, 1 mM DTT, 0.1 mg/ml BSA) in the presence of 16 nM [α-^{32}P]dGTP, 100 μM (dATP, dCTP and dTTP), 100 μM GTP and 100 μM $MnCl_2$ + 4 mM $MgCl_2$ as metal cofactors. After incubation for 30 min at 37°C, the reactions were stopped by adding 50 μl TE and loaded into a G50 + 0.1% SDS to remove free labeled nucleotide. The eluted products were dried and resuspended in 20 μl H_2O. Reactions were run in a 0.8% agarose native gel, dried and exposed for autoradiography. The position of the M13 ssDNA template used (circular and linear form) was determined by ethidium bromide staining of the agarose gel.

EMSA for binary complex and pre-ternary complex

Enzyme:ssDNA binding was performed in buffer A [50 mM Tris–HCl pH 7.5, 40 mM NaCl, 2.5% (w/v) glycerol, 2.5% (w/v) PEG-4000, 1 mM DTT, 0.1 mg/ml BSA], using 5′ PNK-[γ-^{32}P]-labeled 3′T_{20}GTCCT_{36}5′ oligonucleotide (1 nM) and increasing concentrations of either WT PrimPol or W87G, F88L, Y89D, Y90D mutants (10, 20, 40, 80 nM) in the absence of metal. The reaction (in 20 μl) was incubated at 30°C for 10 min. Subsequently, loading buffer (30% glycerol, 1 mM EDTA, 0.1% xylene cyanol and 0.1% bromophenol blue) was added and the reaction was analyzed in a native 6% polyacrylamide gel run at 150 V for 120 min at 4°C in Tris-glycine pH 8.3 buffer. After electrophoresis, the gel was dried and the mobility shift of free ssDNA *vs* enzyme:ssDNA complex was analyzed by autoradiography.

Pre-ternary complex formation of WT PrimPol or W87G, F88L, Y89D, Y90D mutants (1 μM) and labeled nucleotide [α-^{32}P]dGTP or [α-^{32}P]dTTP (16 nM) was evaluated in buffer B [50 mM Tris pH 7.5, 2.5% (w/v) glycerol, 40 mM NaCl, 1 mM $MnCl_2$, 1 mM DTT and 0.1 μg/μl BSA], supplemented when indicated with ssDNA 3′T_{20}GTCCT_{36}5′ (0.5 μM; 60-mer), $MnCl_2$ (1 mM). Reactions (20 μl final volume) were incubated for 10 min at 30°C. Then loading buffer was added and the reactions were analyzed as described above.

DNA polymerase and 8oxoG translesion synthesis assays

For 'standing start' analysis of polymerase activity, a 5′ PNK-[γ-^{32}P]-labeled 15-mer oligonucleotide primer (5′-GATCACAGTGAGTAC-3′) was hybridized to a 28-mer oligonucleotide template (5′-AGAAGTGTATCT(X)GT ACTCACTGTGATC-3′; X stands for G or 8oxoG) and used to evaluate WT PrimPol and the mutated variants (200 nM) in polymerase activity and translesion synthesis in the presence of increasing dNTPs concentrations (1, 10, 100 μM). The reactions (20 μl) in buffer R were incubated at 30°C during 60 min, then stopped and analyzed as described above.

To analyze the fidelity of the active PrimPol variants the insertion of each nucleotide dATP, dCTP, dGTP or dTTP independently at 1 μM opposite the undamaged G and 8oxoG site, was measured. Reactions were incubated at 30°C during 30 min, then stopped and analyzed as described above.

Steady-state kinetics analysis of nucleotide incorporation

Kinetic parameters were obtained by measuring the formation of a +1 primer-extended product by either wild-type PrimPol or by the WFYY mutants F88L and Y89D. Assays contained a 5′ ^{32}P-labeled primer (5′-GATCAC AGTGAGTAC-3′) hybridized to a partially complementary template (5′-AGAAGTGTATCT**C**GTACTCACTG TGATC-3′; C in bold is the first base to be copied). Reactions were carried out (in 20 μl) using Buffer R (50 mM Tris pH 7.5, 5% Glycerol, 75 mM NaCl, 1 mM $MnCl_2$, 1 mM DTT and 0.1 μg/μl BSA), 250 nM primer/template, 40 nM purified WT PrimPol (F88L or Y89D) and increasing concentrations of the first complementary nucleotide, dGTP (from 0.25 to 40 μM). After 10 min incubation at 30°C, reactions were stopped and the products resolved as previously described. +1 primer-extended products were detected using a BAS reader 1500 (Fujifilm). Autoradiographs were quantified by densitometry using ImageJ software. The observed rate of nucleotide incorporation (+1 extended primer) was plotted as a function of nucleotide concentration. Data were fit to the Michaelis–Menten equation using non-linear regression to determine the apparent K_m and k_{cat} parameters.

DNA polymerase and 6-4PP translesion synthesis assays

A 5′ PNK-[γ-^{32}P]-labeled 16-mer oligonucleotide primer (5′-CACTGACTGTATGATG-3′) for 'standing start' 6-4PP TLS experiments was hybridized to either control (undamaged) 30-mer oligonucleotide template (5′-CTCGTC AGCATC(TT)CATCATACAGTCAGTG-3′), or to damaged templates containing an 6-4PP thymine dimer site (6,4), kindly provided by S. Iwai (Osaka University, Japan). The reaction mixture (20 μl) contained buffer R, 1 mM $MnCl_2$, 2.5 nM [γ-^{32}P]-labeled primer/template structure, dNTPs (100 μM) and purified human PrimPol or the WFYY motif variants (200 nM). After incubation for 30 min at 30°C, primer extension products were analyzed as described above.

DNA primase/polymerase assays of Y89D in the presence of Mg^{2+}

As shown in Supplementary Figure S3, the Y89D mutant and the corresponding WT PrimPol (purified from a different source) were tested in different polymerization assays, and in the presence of activating Mg^{2+} ion. A 5′-TET fluorophore-labeled 25-mer oligonucleotide primer (5′- ATAGGGGTATGCCTACTTCCAACTC-3′) was hybridized to 70-mer oligonucleotide template (5′-GAGGGGTATGTGATGGGAGGGCTAGGATATGA GGTGAGTTGAGTGGAGTTGGAAGTAGGCATAC CCCTAT-3′) (27). The reaction mixture (10 μl) contained 10 mM Bis-Tris propane (pH 7.0), 10 mM $MgCl_2$, 1 mM DDT, 200 μM dNTPs, either WT PrimPol or the Y89D

mutant purified as described (24), and PolDIP2 when indicated. After 10 min incubation at 37°C, reactions were stopped by addition of formamide loading buffer (0.5% SDS, 25 mM EDTA, 95% v/v formamide and xylene-cyanol). Products were separated by 7 M urea–containing 10% polyacrylamide sequencing gels, and analyzed by using Typhoon 9400 (Amersham Bioscience) scanner.

The capacity of Y89D to functionally interact with Polγ was tested using M13mp18 ssDNA (New England Biolabs, Ipswich, MA, USA) as a template, as described previously (5,28). The reaction mixtures contained 10 mM Bis-Tris propane (pH 7.0), 10 mM $MgCl_2$, 1 mM DDT, 1 mM ATP and 200 μM dNTPs including [α-^{32}P]dCTP. When indicated 200 nM WT or Y89D PrimPol, purified as described (24), 20 nM PolγA, 30 nM PolγB (as a dimer), and 200 nM PolDIP2 were added. The reaction was performed using 5 nM of primed or non-primed (the 28-mer primer is complementary to M13mp18 nucleotides 6,218–6,245) M13mp18 ssDNA, and after 60 min at 37°C the reactions were stopped with 0.5% SDS/25 mM EDTA, and purified with G-25 columns (GE Healthcare). Products were separated by alkaline (30 mM NaOH, 1 mM EDTA)–1% agarose gel, and analyzed with a Typhoon 9400 scanner.

Circular dichroism (CD) spectroscopy

CD analyses of PrimPol WT and the four WFYY mutants, purified as described (24), were performed on a JASCO J-810 spectropolarimeter (JASCO, Easton, MD, USA) equipped with a Peltier temperature control unit that maintained the temperature at 10°C. A 1 mm quartz cuvette (Hellma, Müllheim, Germany) was used. Before measurements, protein samples were buffer exchanged into a buffer containing 15 mM Tris–HCl (pH 7.5) and 400 mM NaF, and the protein concentrations were adjusted to 0.1 mg/ml. The measurements were made in 5 replicates and averaged in the instrument software. The mean residue ellipticity was calculated using the protein molar concentration and the number of peptide bonds.

Single-molecule analysis of DNA replication in stretched fibers

Stable HeLa-shPrimPol cells were generated by infection of HeLa cells, obtained from the Spanish National Cancer Research Center Repository, with a lentiviral vector carrying a doxycycline (dox)-inducible shRNAmir targeting the sequence 5′ CCTGATGTCTGTGAGATTT 3′ in the 3′ UTR of PRIMPOL gene. Expression of PRIMPOL shRNAmir and downregulation of endogenous PrimPol protein was induced by adding 1 μg/ml dox to the culture medium for 3 days. For functional complementation assays, V5-tagged PrimPol protein (either WT or the indicated mutant derivative) was reintroduced in HeLa-shPrimPol cells by transient transfection of pcDNA3.1/nV5-PrimPol plasmids using Lipofectamine 2000 (Invitrogen), as described (3). To evaluate fork rate (FR), cells were pulse-labeled with 50 μM CldU (20 min) followed by 250 μM IdU (20 min). To evaluate fork restart, cells were pulse-labeled with CldU (red) for 20 min, and irradiated with UV light (30J/m2) for 30 min before pulse-labeling with IdU (green) for 20 min in fresh medium as described (3). Alternatively, 5 mM HU was added to the medium for 6 h between pulses. Labeled cells were harvested and resuspended in 0.2 M Tris pH 7.4, 50 mM EDTA and 0.5% SDS. DNA fiber spreads were prepared as described (3). For immunodetection of labeled tracks, fibers were incubated with primary antibodies (1 h / RT) and the corresponding secondary antibodies (30 min/ RT) in a humidity chamber. In these settings, forks arrested by UV irradiation or dNTP attrition (HU-treatment) should have incorporated only the first analog, whereas those that continued DNA synthesis should be labeled with both analogs. DNA was stained with anti-ssDNA to assess fiber integrity. Fiber images were obtained in a DM6000 B Leica microscope with an HCX PL APO 40× and 0.75 NA objective. The conversion factor used was 1 μm = 2.59 kb. In each assay, >300 tracks were measured for FR estimation and >500 tracks were measured to estimate percentage of fork restart.

Statistical methods

In column graphs, data are expressed as mean ± s.e.m. (standard error of the mean). Statistical analyses were done with two-tailed Student's *t*-test. When the data are presented in scatter dot plots, the bar corresponds to the median value. For the analyses of FR in stretched DNA fibers, the data distribution is normally not Gaussian, and differences between samples were assessed with the non-parametric Mann–Whitney rank-sum test. Statistical analysis was performed in Prism v4.0 (GraphPad Software).

RESULTS AND DISCUSSION

WxxY motif is highly conserved in eukaryotic PrimPols

Amino acid sequence alignment of evolutionarily distant eukaryotic PrimPols from animals and plants allowed the identification of a short amino acid motif, WxxY (Figure 1 and Supplementary Figure S1), in the vicinity of motif A which is universally conserved in all members of the AEP superfamily and contains two metal ligands of the active site (Asp^{114} and Glu^{116} in human PrimPol (4,18), and close to the residue involved in sugar discrimination (Tyr^{100}, 29; green dot in Figure 1 and Supplementary Figure S1). WxxY motif can be more precisely defined as WFYY in vertebrates, and WxRY in plants (where x is frequently a positively charged residue). Thus, collectively, metazoans have a WxxY motif in which the tryptophan (W) is strictly invariant, and the flanking tyrosine is highly conserved (Supplementary Figure S1). Other members of the AEP superfamily, such as putative PrimPols from fungi (*Spu*), archaea (*Pfu*P41, pRN1, *Mhu*, *Sis*) and bacteria (*Tth*, *Taq*, *Mru*, *Msi*1 and *Bc*MCM), and NHEJ polymerases (*Mt*PolDom), do not have a conserved WxxY motif, but most of them conserve the tryptophan, or an equivalent aromatic residue, as the only vestige of this motif (Figure 1).

To understand the role of this conserved motif, we performed site-directed mutagenesis of Trp^{87}, Phe^{88}, Tyr^{89} and Tyr^{90} amino acids of human PrimPol. The changes were designed following different criteria. The most invariant residue of the motif, Trp^{87}, was drastically changed to a

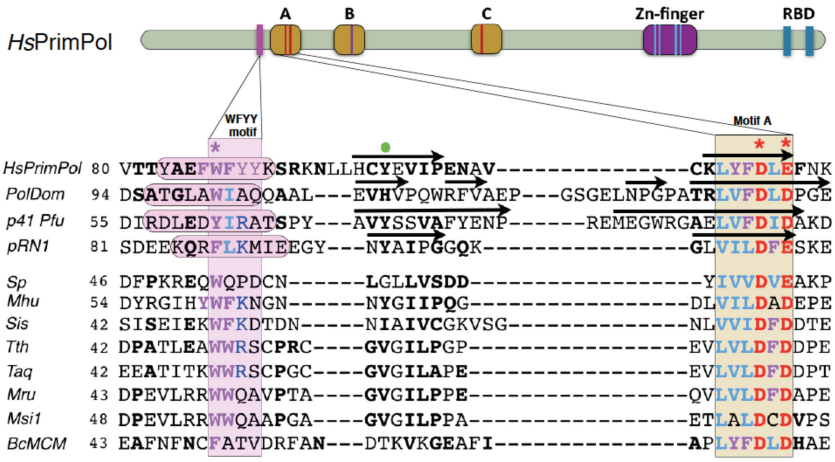

Figure 1. *Hs*PrimPol residue Trp^{87}, embedded in motif WxxY, is conserved among different AEP enzymes. (**Top**) Schematics of human PrimPol showing the position of conserved active site motifs A, B and C, shared by members of the AEP superfamily, a Zn-finger domain similar to that of herpesvirus UL52 primase and the bipartite RPA binding domain (RBD), located at the most C-terminal region. The WFYY motif described in this work (represented as a magenta bar), is proximal to active site motif A. The colored bars inside motifs A and C indicates specific carboxylate residues acting as metal ligands (red), and the specific histidine (purple) involved in nucleotide binding at motif B; blue bars inside the Zn finger domain indicates the cysteines and histidine that coordinate the Zn^{2+} atom. (**Bottom**) Amino acid sequence alignment of an N-terminal segment of different AEP enzymes (spanning from the eukaryotic PrimPol motif WxxY to the universally conserved motif A of AEPs), including *Homo sapiens* PrimPol (*Hs*PrimPol), *Mycobacterium tuberculosis* LigD polymerase domain (PolDom), *Pyrococcus furiosus* primase catalytic subunit (*Pfu*-p41), plasmid pRN1 ORF904 from *Sulfolubus islandicus* (pRN1), and other known or putative PrimPol enzymes in Fungi (*Spicellomyces punctatus (Sp)*), Archea (*Methanospirillum hungatei (Mhu)*; *Sulfolobus islandicus (Sis)*) and Bacteria (*Thermus thermophilus* (*Tth)*; *Thermus aquaticus (Taq*); *Meiothermus ruber (Mru)*; *Meiothermus silvanus (Msi)*; PrimPol-helicase from *Bacillus cereus (BcMCM)*). Some selected human PrimPol residues are indicated: Tyr^{100} (sugar discriminator; green dot); Asp^{112} and Glu^{114}, (acting as metal ligands in motif A; red asterisks); Trp^{87} (as part of the WFYY; magenta asterisk). The secondary structure elements, obtained from their corresponding 3D-structures (*Hs*PrimPol, PolDom, *Pfu*-p41 and pRN1), are indicated with cylinders (alfa-helices) and arrows (beta strands) above the corresponding amino acid sequence.

glycine (W87G) to abolish the aromatic ring and its potential function. Phe^{88}, invariant in PrimPols from vertebrates as part of their WFYY motif, was changed to leucine, mimicking a human PrimPol variant (F88L). Tyr^{89}, invariant in PrimPols from vertebrates as part of their WFYY motif, was changed to aspartate to further study a mutant (Y89D) that has been controversially associated with High Myopia (20,21,23) and PEO (22). Finally, the highly conserved Tyr^{90} was changed to aspartate (Y90D), mimicking the natural mutation in Tyr^{89}, which eliminates its volume and aromaticity but introducing a negatively charged residue.

Trp^{87} and Tyr^{90} residues of human PrimPol are essential for its DNA primase activity

To evaluate the possible effects of the point mutations introduced at the WFYY motif on the function of human PrimPol, we performed a highly-specific primase *in vitro* assay, which measures *de novo* formation of short primer products at a single priming site (4). In this assay, a single-stranded DNA oligonucleotide containing a preferred priming site ('GTCC') flanked by poly T residues (Figure 2A) was used as a template in the presence of [γ-^{32}P]ATP as the 5′-nucleotide, increasing concentrations of dGTP as the incoming 3′-nucleotide, and activating Mn^{2+} ions. Under these conditions, WT PrimPol gave rise to the expected products *3pA*dG, *3pA*dGdG, together with longer products (*3pA*dGdGdG, *3pA*dGdGdGdG,….) due to reiterative dG addition *via* slippage (Figure 2A, lanes 2-4). Interestingly, the changes made at the two invariant residues of the motif (W87G, Y90D) virtually eliminated the primase activity (Figure 2A, lanes 5–7 and 14–16), demonstrating that Trp^{87} and Tyr^{90} in human PrimPol's WFFY motif are essential for dimer synthesis. The histogram at Figure 2A, showing the quantification of the primase activity at 100 μM dGTP, indicates that variant F88L retains only 25% of the WT activity. The effect is even more pronounced when using 10 μM dGTP (compare lanes 3 and 9; 20% residual activity) or 1 μM dGTP (compare lanes 2 and 8; 5% activity remaining). Note that the F88L mutant required about 100-fold higher concentration of dGTP than WT PrimPol to produce a similar pattern of initiation products (compare lanes 2 and 10). Conversely, the primase activity of the Y89D variant was only slightly reduced (60-65% of WT PrimPol), and was not affected by the dGTP concentration used (Figure 2A, lanes 11–13).

The effect of these mutations on the primase activity was further analyzed by using a slightly modified oligonucleotide as template (now having a 'GTCA' priming site) to dissect the dimer formation step that is rate-limiting during primer synthesis, and its further elongation to synthesize a longer primer (Figure 2B). Dinucleotide formation was evaluated by providing a high concentration (100 μM) of *ATP*, which is valid as 5′-site nucleotide, but a very low concentration (16 nM) of labeled [α-^{32}P]dGTP as the 3′-site nucleotide. Progression from initiation to elongation was assayed by providing 100 μM dTTP, which allows trinucleotide formation (3*pA*dGdT) and subsequently elongation via *ATP* incorporation. As expected from the previous assay, both W87G and Y90D mutants were unable to form the initial dinucleotide also in these conditions; consequently, elongated primers were also not detectable

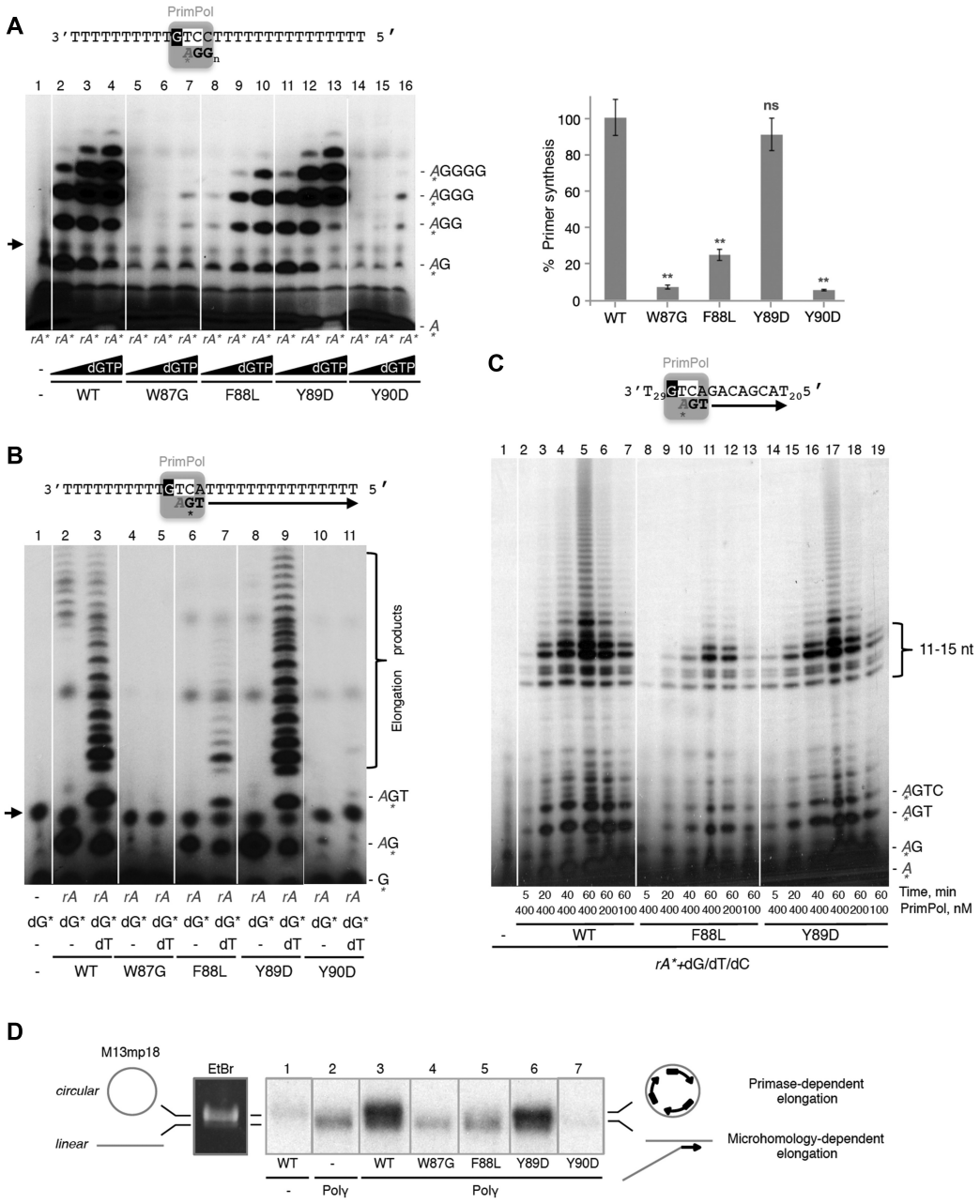

Figure 2. Trp^{87} and Tyr^{90} human PrimPol residues are required for its primase activity. (**A**) Primase assay using an ori-containing oligonucleotide (GTCC; 1 μM) as template, WT or mutant *Hs*PrimPol (400 nM), $MnCl_2$ (1 mM), labeled [γ-^{32}P]*ATP* (16 nM) as the 5′-site nucleotide, and dGTP (1, 10, 100 μM) as the 3′-site nucleotide. The autoradiogram shows the expected *A**G and *A**GG, and other extension products generated by reiterative insertion of dGTP (4). Relative quantitation of primer synthesis at 100 μM dGTP, carried out by optical densitometry and normalized to 100% WT, is shown at the right. In all cases, the histograms represent the mean ± SEM (standard error of the mean) from three different experiments. Data significance were analyzed using Student's t test (ns, not significant > 0.05, ***P* < 0.01). (**B**) Primase assay using a slightly modified template (GTCA; 1 μM); in this case, providing *ATP* (100 μM) and [α-^{32}P]dGTP (16 nM), and dTTP (100 μM) when indicated. As in part A the reactions were analyzed by 8M urea /PAGE and autoradiography, as described in Materials and Methods. Under these conditions, dimer (*A**G), trimer (*A**GT), and further elongated products (*A**GTA_n) could be observed. Arrowheads indicate non-specific bands that are observed even in the absence of PrimPol (lanes 1 in parts A and B). (**C**) Assay to measure processivity during primer synthesis, using a template with the preferred priming site (3′GTC) followed by an heterologous sequence (3′T$_{29}$**GTC**AGACAGCAT$_{20}$ 5′), in the presence of 16 nM [γ-^{32}P]ATP and dGTP, dCTP and dTTP, each at 100 μM each. Under these conditions, long primers are formed either with WT PrimPol or mutants F88L and Y89D, at any time point and enzyme concentration. (**D**) Synergy between human PrimPol and mitochondrial Polγ. The primase capacity of WFYY mutants (100 nM) was evaluated in combination with mitochondrial Polγ (20 nM), and using M13 ssDNA (5 ng/μl) as template. After incubation for 30 min at 37°C as indicated in Materials and Methods, the reactions were analyzed by native agarose gel electrophoresis and autoradiography. The selected images are representative of at least 3 different experiments. Ethidium bromide staining of the M13 template used shows the mobility of a prominent upper band (circular form), and that of a weak lower band (linear form). The schematics at the right indicate the origin of different labeled products: the upper product is obtained when PrimPol makes primers on the circular DNA, which can be further extended by Polγ; the lower product, generated by Polγ alone, corresponds to 3′-extension products of the linear form, most likely after microhomology pairing of two M13 molecules.

(Figure 2B, lanes 4–5 and 10–11). Also, in congruence with the previous assay, mutant Y89D was able to catalyze extensive elongation of the dimers at a slightly higher efficiency (130%) than the WT PrimPol (Figure 2B; compare lanes 3 and 9). On the other hand, the F88L variant displayed a reduced efficiency (19% of WT activity) to form the elongated primers (Figure 2B, compare lanes 3 and 7).

At this point we could not rule out that the effect of the mutations introduced could be template-specific. Thus, we used a ssDNA template with a preferred initiation site (3′GTC) followed by an heterologous sequence which precedes a polyT tail (Figure 2C). PrimPol is allowed to start DNA synthesis with [γ-^{32}P]ATP (16 nM) and dGTP (100 μM), forming a *3pA*G dimer, which can be elongated up to *3pA*GTCTGTCGT in the presence of dTTP, dCTP, and dGTP (100 μM each). Primer synthesis by WT *versus* F88L and Y89D mutants was compared as a function of time (5-60 min). This experiment showed that Y89D priming efficiency was only slightly affected (58–64%), at any reaction time (Figure 2C, compare lanes 2–5 versus 14–17). On the other hand, the reduced efficiency of F88L mutant in primer synthesis was more evident at lower reaction times (Figure 2C, compare lanes 2–5 versus 8–11; i.e. 10% at 20 min (lane 9) versus 21% at 60 min (lane 11). Interestingly, this experiment shows that WT Primpol makes products of similar size at any time point (Figure 2C, lanes 2–5), and also at different enzyme:DNA ratios (Figure 2C, lanes 5–7), which supports our previous finding that PrimPol is processive when making primers (11), unlike the distributive behavior observed when assayed as a polymerase on conventional primer/template substrates. PrimPol's processivity when priming is unaffected by mutations F88L and Y89D (Figure 2C, lanes 8–13 and lanes 14–19, respectively).

Finally, we compared the overall capacity of WT PrimPol and the WFYY mutants to generate primers in a large heteropolymeric template sequence (M13 ssDNA), and whether they can be efficiently extended by DNA polymerase gamma (Polγ), the mitochondrial replicase (30,31). In this template context, PrimPol primase activity is evaluated as an average of different events occurring at preferred and non-preferred initiation sites. Importantly, the analysis of the reaction is carried out by agarose gel electrophoresis under native separation conditions, thus preserving the association of the nascent and labeled products with the intact circular template (M13ssDNA). As shown in Figure 2D (lane 2), a lower/faster migrating band running at the position of linear (nicked) M13 ssDNA (stained with EtBr) was observed when only providing Polγ (in the absence of a primase), suggesting that labeling is due to the extension of the linearized 3′-end, acting as primer after hybridization to a (partially) complementary DNA sequence (see schematic at the right). The upper band corresponds to the mobility of circular ssDNA M13, and therefore, any labeling is the consequence of *de novo* priming by PrimPol, followed by processive elongation by Polγ. As shown in Figure 2D, only WT PrimPol (lane 3) and mutant Y89D (lane 6) were able to make DNA primers, as judged by their efficient extension by Polγ and quantification of the upper band (Figure 2D). Again, F88L displayed low primer synthesis ability (lane 5), with only 27% of the WT activity. In agreement with previous data, W87G and Y90D mutants were unable to produce DNA primers (lanes 4 and 7, respectively), thus preventing any extension reaction by Polγ.

In conclusion, the defects shown in primase activity correlate well with the conservation of each individual residue in the WFYY motif, outlining that the invariant residues Trp^{87} and Tyr^{90} of human PrimPol are essential to initiate dinucleotide formation during primer synthesis.

Trp^{87} and Tyr^{90} residues are crucial to form a stable pre-ternary complex

To further investigate why these conserved residues are essential for the primase activity, we studied their importance in ssDNA binding. Electrophoretic mobility shift assays (EMSA), carried out at different enzyme:ssDNA ratios, demonstrated that each mutant at the WFYY motif was able to produce a binary complex with ssDNA (E:DNA) with the same electrophoretic mobility as WT PrimPol, and also with similar efficiency (Figure 3A). The capacity of WFYY mutants to form the binary complex and their similar mobility also argues against a significant change in the overall structure of PrimPol that could be caused by the mutations. To confirm this, CD-spectra for all the mutants were obtained, confirming the absence of significant structural alterations (Figure 3B). Consequently, as the WFYY motif of human PrimPol is irrelevant for binding to ssDNA, the conserved residues Trp^{87} and Tyr^{90}, and to a lower extent Phe^{88}, should be required in a later step of the priming reaction (revised in 12).

As described before, PrimPol recognizes the G in the 'GTCC' core sequence as a cryptic nucleotide and forms the initial dimer (*3pA*dG) in front of T and C (4): the 3′site nucleotide (dGTP) is the one that binds first, forming the so-called 'pre-ternary complex' PrimPol:ssDNA:dGTP in the presence of Mn^{2+} ions; the second nucleotide (deoxi or ribo ATP) gets bound at the 5′ position once the 3′ site is occupied (11,12). We evaluated the formation of the E:DNA:dG preternary complex by WFYY mutants and found that F88L (Figure 3C, lane 6) and Y89D (Figure 3C, lane 8) variants could form the pre-ternary complex albeit less efficiently (F88L, 40% and Y89D, 60%) than WT PrimPol (Figure 3C, lane 2). Conversely, W87G and Y90D mutants were completely unable to bind the incoming nucleotide at the 3′-site required to form the preternary complex (Figure 3B, lanes 4 and 10, respectively), thus explaining their inactivity in the primase assays.

Base insertion fidelity operates during formation of the pre-ternary complex, as the bound 3′-site nucleotide is preferentially complementary to the templating base (11), implying its stabilization via Watson & Crick base pairing. Pre-ternary complex formation was also tested in the presence of an incorrect 3′-site nucleotide (dTTP) to investigate whether the impaired function of mutants F88L and Y89D could be due to an altered orientation of the templating base that could be beneficial for a non-complementary nucleotide. However, WT PrimPol as well as the partially active variants F88L and Y89D formed only small amounts of pre-ternary complex with dTTP as a non-complementary nucleotide (Figure 3C, light grey bars in the histogram). The estimated ratio of correct *vs* incorrect pre-ternary complexes was similar for WT PrimPol (>10.3) and variants

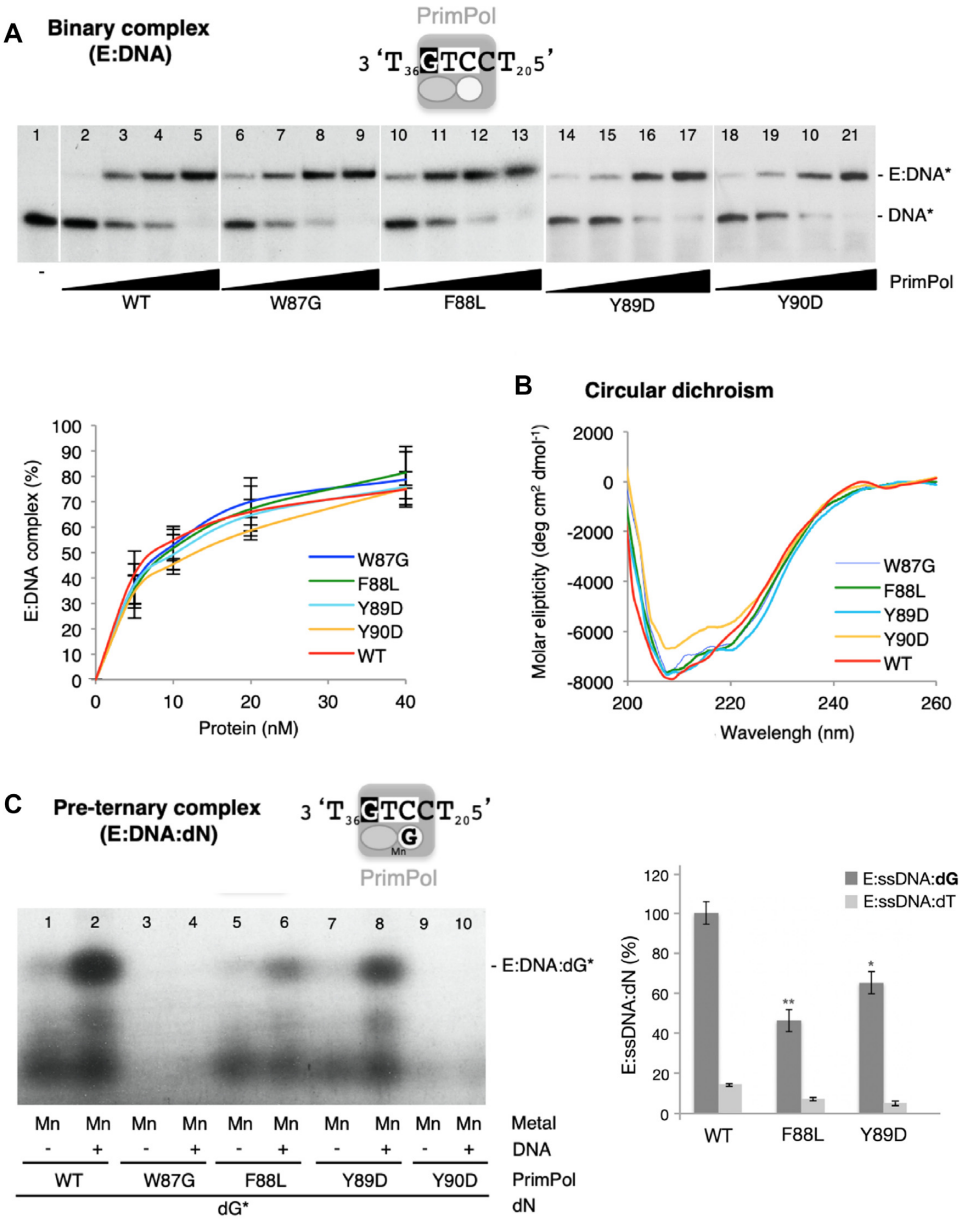

Figure 3. The WFYY motif of human PrimPol is required to stabilize the preternary complex. (**A**) Binary complex detected by electrophoretic mobility shift assay (EMSA) using oligonucleotide GTCC (2.5 nM) (60-mer; [γ-^{32}P]-labeled), and increasing concentrations of WT PrimPol or mutant variants (5, 10, 20, 40 nM). The retarded band detected by autoradiography (upper panel) corresponds to the E:ssDNA binary complex. The lower panel shows the quantification (average of three different experiments) of the E:ssDNA complex by optical densitometry, expressed as percentage of the labeled ssDNA. (**B**) Circular dichroism (CD) spectra of PrimPol WT and WFYY mutants, purified as described (24). CD analyses were performed on a JASCO J-810 spectropolarimeter (JASCO, Easton, MD, USA), as described in more detail in Materials and Methods. The mean residue ellipticity was calculated using the protein molar concentration and the number of peptide bonds. The graph shows that the overall structure of W87G, F88L, Y89D and Y90D mutants is preserved. (**C**) Pre-ternary complex detected by EMSA, using [α-^{32}P]dGTP (16 nM) and PrimPol WFYY variants (1 μM) with 3′T$_{36}$GTCCT$_{20}$5′ (500 nM) as ssDNA template in the presence of Mn^{2+} (1 mM). The histogram represents the quantification of the preternary complex (E:ssDNA:dNTP) formed, carried out by optical densitometry (normalized to 100% WT) of the preternary complex with the complementary (dGTP; dark gray bars) or non-complementary (dTTP; light gray bars) nucleotide. In all cases, the histograms represent the mean ± SEM (standard error of the mean) from three different experiments. Statistical data analysis for the correct preternary complex (E:ssDNA:dG) was carried out using Student's *t* test (*$P < 0.05$ and **$P < 0.01$) for each WT/mutant pair.

F88L (>11.7), Y89D (>10.9), suggesting that these mutations do not alter the fidelity of nucleotide selection to form the pre-ternary complex, but its efficiency.

Trp^{87} and Tyr^{90} residues are essential for PrimPol DNA polymerase activity

When the WFYY mutants were tested in conventional DNA polymerase assays, using a pre-formed template/primer hybrid and different concentrations of dNTPs, the results mirrored those shown for primase activity (Figure 4A, left panel). Thus, W87G and Y90D mutants were inactive, F88L activity was significantly reduced, and Y89D had a near to wild-type like activity. Besides, the latter two mutants did not show a significant alteration in the fidelity of nucleotide incorporation, evaluated here by comparing the preferred nucleotide for the + 1-insertion reaction opposite dG (Figure 4B, left panels).

The reduced or null ability of some of the WFYY mutants to form the pre-ternary complex (as shown in Figure 3C) suggests that the parallel defects observed in DNA polymerization are also due to a lower affinity for the incoming 3′-site dNTP, that compromises the formation of the ternary complex required for each polymerization cycle. To test this idea, we determined the steady-state kinetic parameters of the active variants F88L and Y89D during a single nucleotide incorporation polymerization, which can reveal differences that might not be apparent in the primer extension assay. The reduction in the catalytic efficiency of variants F88L (7,5-fold lower than WT) and Y89D (4,3-fold lower than WT) was mainly due to a reduction in the affinity for the incoming dNTP in the case of F88L (4.5-fold higher K_m than WT; 1.5-fold lower k_{cat} than WT), but mainly due to a reduction in k_{cat} in the case of Y89D (1.5-fold higher K_m than WT; 3-fold lower k_{cat} than WT; Table 1).

Besides catalyzing conventional DNA-directed DNA synthesis, PrimPol bypasses 8oxoG lesions during polymerization with high efficiency, inserting dATP slightly better than dCTP when Mn^{2+} is used as metal activator (4,17,18). As shown in Figure 4B (right panels), when the template contained an 8-oxo-G lesion, the WFYY mutants activity mirrored the previous results obtained with the undamaged template: mutants W87G and Y90D mutants were inactive, whereas F88L and Y89D had reduced polymerization activity but still elongated the primer across the damaged base as efficiently as they did with the undamaged template (compare Figure 4A, left and right panels). Similar to WT PrimPol, F88L and Y89D variants inserted the correct (dCTP) and pre-mutagenic (dATP) nucleotides at similar ratios opposite 8oxoG, whereas dGTP and dTTP were incorporated at a much lower extent (Figure 4B, middle and bottom panels).

Therefore, these data support the importance of the invariant residues of the WxxY motif (Trp^{87} and Tyr^{90} in human PrimPol) in nucleotide binding also during polymerase reactions on either undamaged or damaged DNA templates. On the other hand, the F88L and Y89D variants do not influence the TLS ability of PrimPol, keeping the WT-like dC/dA insertion ratio when copying an 8oxoG lesion.

The F88L variant is defective in alternative TLS reactions on UV-damaged DNA

PrimPol bypasses UV lesions in the DNA template by also using alternative TLS mechanisms based on template distortions and primer realignment (3,16). We assessed the TLS activity of WFYY mutants on 6,4 pyrimidine-pyrimidone (6,4PP), a characteristic lesion caused by UV irradiation. As expected, the W87G and Y90D mutants were inactive, both on the undamaged (control) or damaged template structures (Figure 5A and B). On the other hand, mutant Y89D behaved essentially as the WT PrimPol: (i) reaching full-length extension of the primer (+14) when using the control undamaged template/primer structure (Figure 5A); (ii) producing a main shorter product (+8) when the template contains the 6,4PP lesion, which requires microhomology-based realignment of the primer ahead of the lesion (3), as indicated in the schematic (Figure 5B). F88L variant copied the undamaged control template less efficiently than WT PrimPol (Figure 5A), which only partially explains the strong reduction of the +8-product generated on the 6,4PP-containing template (Figure 5B). This suggests that the F88L variant defect, which reduces its polymerization capacity, is especially deleterious when TLS requires the realignment of the primer beyond the lesion.

It could be possible that a deficient formation of the ternary complex during each polymerization cycle would be rate-limiting under conditions requiring template or primer dislocation. A plausible explanation is that this 'pseudo-TLS' reaction probably requires the formation of a stable pre-ternary complex beyond the lesion, to trigger primer realignment as a second step. The Y89D variant did not have a significant defect to perform this 'pseudo-TLS' reaction, in agreement with its competence to bind the incoming 3′-site nucleotide. Conversely, the very low activity of the F88L variant is compatible with its poor capacity to form a stable pre-ternary complex (Figure 3B and C).

Mutations at motif WFYY of human PrimPol impair replication fork restart

At the time of the initial characterization of human PrimPol in 2013, it was described that PrimPol downregulation slows down fork progression, suggesting that it plays a basal role during unperturbed DNA replication (3,13). Moreover, PrimPol is actively recruited to rescue DNA synthesis at stalled replication forks challenged by UV irradiation, hydroxyurea (HU; 3,5), or other kind of replication roadblocks (14,32). PrimPol-dependent fork stalling could be rescued by reintroducing wt-PrimPol in the cells, but not the catalytically-dead variant AxA that lacks two of the three catalytic metal ligands (Asp^{114} and Glu^{116}), or a primase-deficient PrimPol lacking the Zn-finger domain (3). To validate the results obtained *in vitro* with the different mutants at the WFYY motif of human PrimPol, we used stretched DNA fiber analysis to measure fork rate (FR) in functional complementation assays, downregulating the expression of endogenous PrimPol and reintroducing the W87G, F88L, Y89D, Y90D mutant versions. The expression levels of V5-tagged WT PrimPol and WYFF mutant versions were approximately similar, and their subcellular distribution in HeLa cells was not affected (Supplementary Figure S2). In

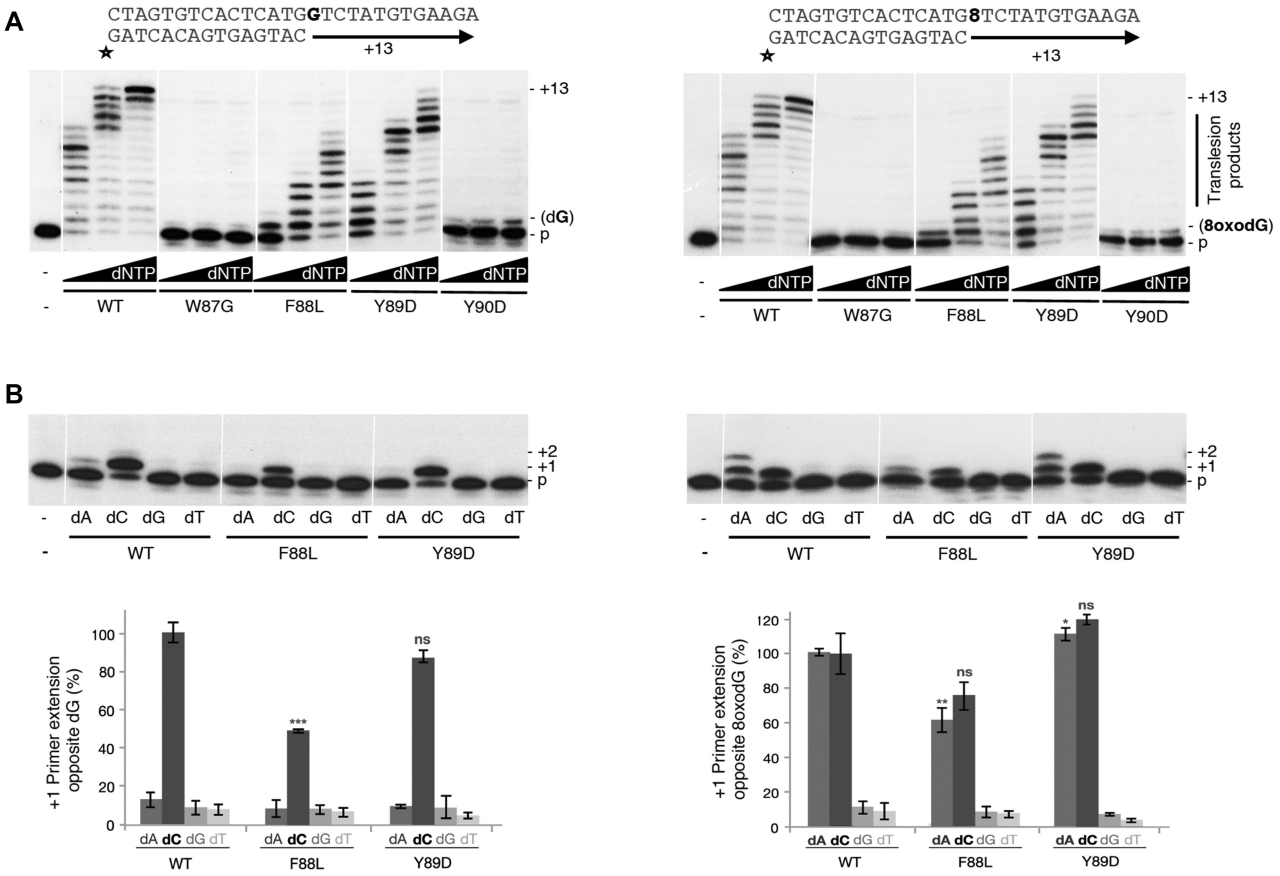

Figure 4. Trp^{87} and Tyr^{90} residues are essential for PrimPol polymerase activity. (**A**) Standing-start polymerization by human PrimPol and WFYY mutants (200 nM) on an undamaged template (X = G; left panel) or on a template containing an 8oxoG lesion (X = 8oxoG; right panel). dNTPs were added in increasing concentrations (1, 10, 100 μM) in the presence of 1 mM $MnCl_2$. (**B**) Standing-start polymerization assay using 2 nM of a template containing either a template G (left panel) or an 8oxoG lesion (right panel), and providing 200 nM of either WT PrimPol or F88L, Y89D variants. dNTPs were individually added at a concentration of 1 μM. The histogram shows the quantification of the reactions shown in part B, obtained by densitometry of the bands corresponding to the extended primer. In all cases, the histograms represent the mean ± SEM (standard error of the mean) from three different experiments. Statistical data analysis for the correct dC insertion opposite dG, and for the two alternative insertions (dA and dC) opposite 8oxodG, was performed using Student's *t* test (ns, not significant > 0.05, *$P < 0.05$, **$P < 0.01$ and ***$P < 0.001$) for each WT/mutant pair.

Table 1. Steady-state kinetic parameters of dGTP insertion by WT PrimPol *versus* F88L and Y89D variants. Data are means (± standard error) from at least three independent experiments

Protein	Template	dNTP	K_m (μM)	K_m (WT/mutant)	k_{cat} (s^{-1})	Cat. eff. (s^{-1} μM^{-1})	Cat. eff. (WT/mutant)
WT	dC	dGTP	0.97 ± 0.08	1	(3 ± 0.003) x 10^{-3}	3 × 10^{-3}	1
F88L	dC	dGTP	4.37 ± 0.96	4.5	(2 ± 0.006) x 10^{-3}	4 × 10^{-4}	7.5
Y89D	dC	dGTP	1.45 ± 0.47	1.5	(1 ± 0.005) x 10^{-3}	7 × 10^{-4}	4.3

good agreement with *in vitro* data, W87G and Y90D mutants lacking primase and polymerase activity were unable to reverse the effect of PrimPol loss on FR, W87G being as inefficient as the AxA catalytically-dead mutant (Figure 6A). Conversely, F88L and Y89D variants rescued FR at the same level as the reintroduction of WT PrimPol, suggesting that their remaining activity is sufficient to sustain the normal range of FR under unperturbed conditions (Figure 6A).

Under DNA replication stress (RS) induced by UV or HU treatment, RNAi-mediated downregulation of endogenous PrimPol levels produces a significant drop in the fraction of restarted forks, which can be complemented only by a primase-proficient PrimPol (3). During UV treatment, RS is caused by the formation of pyrimidine dimers among other lesions created that increase the frequency of fork stalling. In the case of HU, RS is produced by a decrease in the available pools of dNTPs. Again, in agreement with the *in vitro* data, when the two most conserved residues of the WFYY motif (Trp^{87} and Tyr^{90}) are mutated, the capacity of PrimPol to sustain repriming and rescue of stalled forks *in vivo* is lost (Figure 6C). Again, the Y89D variant was as efficient as WT PrimPol to rescue stalled forks under both treatments (UV, HU), which correlates well with its WT-like primase and TLS activities (Figure 6B, C). Interestingly, the human polymorphic variant F88L was unable to fully res-

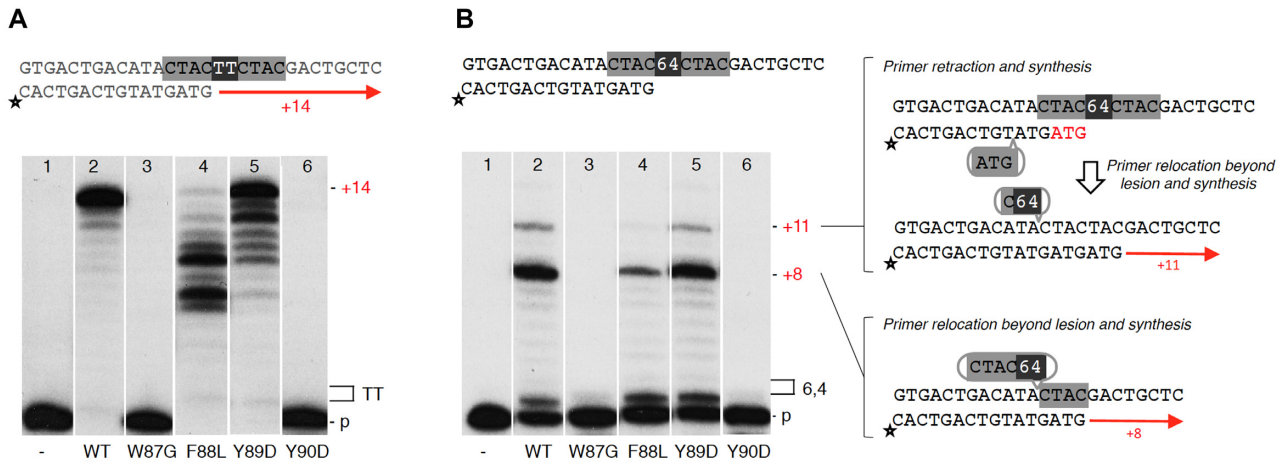

Figure 5. F88L variant is defective in TLS reactions on UV-damaged DNA. (**A**) DNA polymerization assay on a control (undamaged) template. (**B**) DNA polymerization assay on a template containing a 6-4 PP lesion where + 8 and + 11 bands are produced after primer realignment (3,16), as indicated in the schematics. The reactions contain 100 μM dNTPs, 2 nM DNA, 1 mM $MnCl_2$, and 200 nM of either WT or F88L, Y89D variants. The selected images are representative of at least three different experiments.

cue the stalled forks after UV-damage or upon HU treatment (Figure 6C), probably due to its reduced 3′ nucleotide binding, that affects both its primase activity and its TLS abilities to avoid/skip UV-lesions as 6,4 PP, as previously shown.

These experiments demonstrate that the WFYY motif of human PrimPol is relevant for its *in vivo* function, and show an excellent agreement with the results obtained *in vitro*. Of note, the data shown here do not indicate any loss of functionality for mutant Y89D in human cells, which is in contrast with previous results (21) and might also questions the link of this specific mutation with High Myopia (20) and PEO (22). On the other hand, our analysis of the F88L mutant indicates a reduced enzymatic potential of this human PrimPol variant for its contribution to minimize DNA replication stress.

Structural basis for the defective 3′nucleotide binding associated to mutations at the WFYY motif

The crystal structure of human PrimPol in complex with both DNA and incoming 3′dNTP (PDBid: 5L2X; 19; see Figure 7A) provides valuable information to infer the role of the WFYY motif. As shown in Figure 7B, Trp^{87} can establish Van der Waals interactions with Phe^{327} (located in α-helix 6; depicted in green), whose relevance is supported by the invariant presence of this residue in PrimPols from animals and plants; a nearby aromatic residue in human PrimPol, Tyr^{324}, can also establish complementary interactions with Trp^{87}, and its neighbor residue Glu^{323} makes a polar interaction with Tyr^{293} (located at the loop after ß-strand 11; depicted in brown). Strikingly, Tyr^{293} and Ser^{295} directly interact with Tyr^{90} of the WFYY motif. Moreover, these two residues Trp^{87} and Tyr^{90} also make mutual contacts.

In light of the results obtained by mutational analysis of WFYY motif, which outlined the importance of Trp^{87} and Tyr^{90} in binding the incoming 3′-site nucleotide, our hypothesis is that the network of interactions maintained by these two residues, that would be lost by W87G and Y90D mutations, is crucial to induce a large torsion in ß-strand 11 (indicated with an arrow in Figure 7B) that keeps the appropriate orientation of the catalytic Arg^{291} and perhaps that of other residues as Lys^{297} and Lys^{300}, to allow their stabilizing interactions with the 3′-incoming nucleotide via the 3′-OH group and the triphosphate moiety (see Figure 7B, and the scheme in Figure 7C). Moreover, a precise orientation of Arg^{291} is also needed to allow its interaction with the invariant Ser^{167}, invariant at motif B in AEPs (Figure 7B, C).

The crystal structure (19) also shows that Phe^{88}, not strictly conserved at the WFYY motif, interacts with Glu^{85} via its main chain (Figure 7B,C). Glu^{85} directly contacts Trp^{42}, and an alteration of this interaction due to the F88L mutation could modify the orientation of residues His^{46}, Arg^{47} and Gln^{48} that are crucial in the positioning of the templating base (shown in red in Figure 7B). The F88L mutation did not affect the overall interaction with the ssDNA template (Figure 3A), and had a WT-like CD spectrum (Figure 3B), suggesting unaltered overall protein structure. Still, the orientation of the templating base could be affected, explaining the reduced formation of the pre-ternary complex (Figure 3B,C) and the lower affinity for the incoming nucleotide during polymerization (Table 1). Alternatively, the lack of the aromatic ring in the F88L mutation could alter the interaction network involving Trp^{87} and Tyr^{90}, thus partially affecting the capacity to bind the 3′-site incoming nucleotide. Interestingly, the reduced activity of the F88L variant was able to sustain a normal fork rate but failed to restart stalled replication forks after stress, a difference that could be valuable for prognosis of those cancers characterized by high levels of replication stress (33).

The crystal structure of human PrimPol also shows that Tyr^{89}, moderately conserved at the WFYY motif, can establish Van der Waals interactions with the close residue Phe^{86} (via its main chain and phenyl ring) and also with Trp^{42} (via their aromatic moieties). Phe^{86} also interacts with its neighbor residue Glu^{85}, which in turn can also inter-

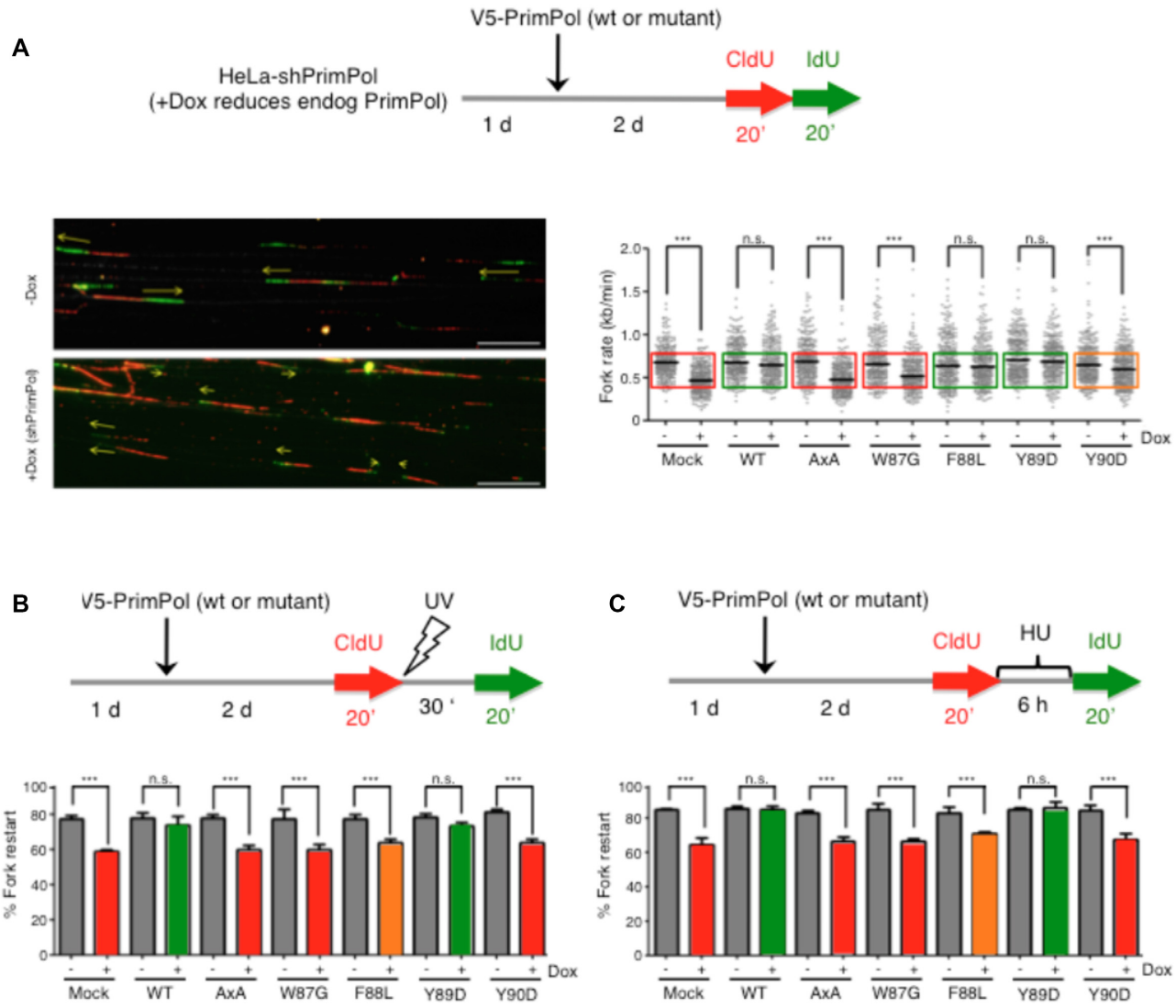

Figure 6. The WFYY motif of human PrimPol is crucial to maintain an optimal replication fork rate and to reprime stalled forks after replicative stress. (**A**) PrimPol Trp^{87} and Tyr^{90} are required to maintain the replication fork rate in S-phase. The schematics outline the workflow of the experiment (see Materials and Methods). Fork rate (FR) values were calculated from stretched fibers corresponding to unperturbed DNA replication of HeLa-shPrimPol cells with or without doxycycline treatment. Microscopy images show representative pictures of the DNA fibers with (–Dox) and without (+Dox) endogenous PrimPol (scale bar 10 μm), performed as described (3) When indicated, plasmids encoding V5-tagged WT, AxA or WFYY mutants were transfected into HeLa-shPrimPol cells (N = 2), to evaluate their capacity to complement the absence of the endogenous PrimPol. N forks > 300; n.s. = not significant, ***$P < 0.001$ (Mann–Whitney test). (B, C) Trp^{87}, Phe^{88} and Tyr^{90} residues are necessary to reprime UV-stalled (**B**) and HU-stalled (**C**) forks**.** The schematics outline the workflow of the experiments (see Materials and Methods). Histograms show the quantification of the percentage of fork restart upon UV-irradiation (**B**) or HU treatment (**C**) in HeLa-shPrimPol cells with or without Dox treatment (performed as described in reference 3). When indicated, plasmids encoding V5-tagged WT, AxA or different point WFYY mutants were transfected. ($N = 2$) to evaluate their capacity to complement the reduction of rescued forks (N structures = 500) caused by the absence of the endogenous PrimPol ($N = 2$). One-way ANOVA and Bonferroni post-test were applied, *** $P < 0.0001$, n.s.: not significant.

acts with the aromatic ring of Trp^{42}. Modeling of the Y89D mutation in the 3D-structure showed that the Asp residue can make similar interactions with Phe^{86} and Trp^{42}, and a polar contact with Tyr^{90} via its main chain. Therefore, the Y89D mutation appears to be structurally conservative, explaining the moderate effect of this alteration on PrimPol *in vitro* activities and the absence of an effect on the tested PrimPol *in vivo* activities. Interestingly, a single mutation of Tyr^{89} to Arg (Y89R), a change that is invariantly present in the WxRY motif of plant PrimPols (see Supplementary Figure S1), enhanced the capacity of human PrimPol as an efficient RNA-dependent-DNA primase/polymerase (34). Strikingly, this randomly selected mutation (Y89R) displayed an increased stabilization of the preternary complex (protein:template DNA:incoming nucleotide), the specific step preceding dimer formation.

Overall, the 3D structural model allows to infer that the WxxY motif conserved in eukaryotic PrimPols has an indirect but fundamental role in stabilizing the 3′-incoming dNTP, in order to form a pre-ternary complex which is crucial for both primase and TLS polymerase activities.

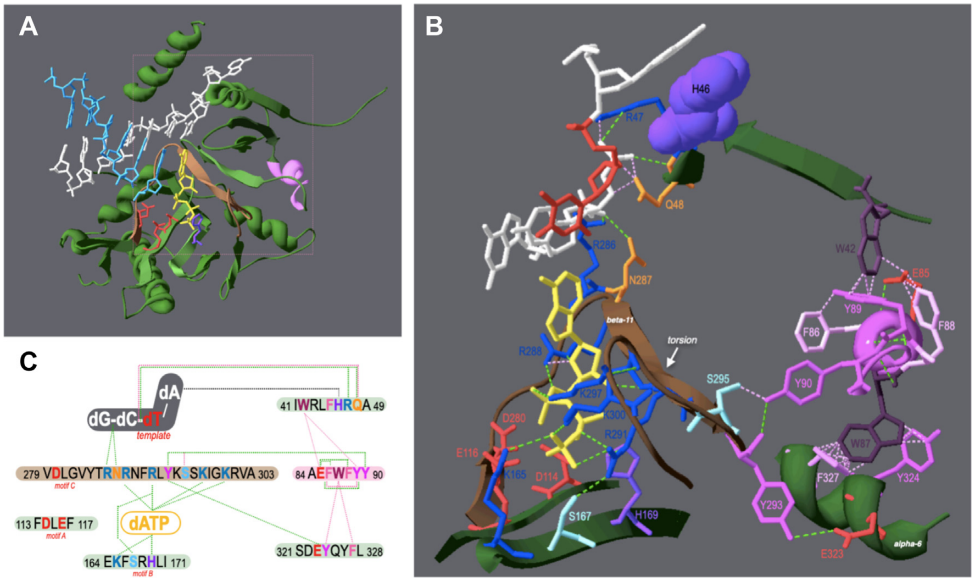

Figure 7. Structural basis for the defective 3′-nucleotide binding associated to mutations at the WFYY motif**.** (**A**) Ribbon representation of the quaternary complex of *Hs*PrimPol:DNA:dATP (PDB id: 5L2X; 19), depicting the interaction of PrimPol (green) with DNA (primer strand is colored cyan, and templating strand in white) and dATP (yellow). Residues of motifs A and C acting as metal ligands (Asp^{114}, Glu^{116}, Asp^{280}) are indicated in red, and the invariant histidine (H169) of motif B is indicated in purple. The amino acid segment spanning residues 279 to 303 is colored brown, and the small alpha helix (residues 84–90), containing the WFYY motif, is colored in pink. (**B**) Enlarged view of the region boxed in A, showing specific residues interacting with the 3′-incoming nucleotide (in yellow), and with the templating DNA (in white/red); moreover, other amino acid residues (mostly aromatic) forming an interaction network with residues of the WFYY motif are also highlighted (see text for details). The arrow indicates the torsion at the ß-strand 11(in brown), likely maintained by a network of interactions involving the WxxY motif. (**C**) Schematics of the different interactions affecting the template and incoming 3′-deoxynucleotide, involving the WFYY motif and other segments of the PrimPol 3D-structure.

Mutation Y89D in human PrimPol is not supportive of a correlation with High Myopia

Despite the importance of PrimPol in damage tolerance during DNA replication, its association with human disease remains largely unknown. In 2013, a study of exome sequencing described that a point mutation in PrimPol, Y89D (located at the WFYY motif studied here), correlated with the development of High Myopia in human patients (20). The following year, another study claimed that the Y89D mutation negatively affected the DNA binding capacity and enzymatic activities of PrimPol (21); this report also described that the Y89D mutation induced structural changes in PrimPol and therefore, its lower activity *in vitro and in vivo* was correlated with an inefficient protein folding. In contrast, our structure-function analysis shows that the predicted pathological mutation Y89D does only mildly affect the activity of PrimPol *in vitro*. To reinforce our conclusions, we tested a Y89D protein obtained with a different expression and purification method (see Supplementary Figure S3). This alternative Y89D mutant protein again showed a near to WT PrimPol-like activity in DNA polymerase assays, in spite of using different assay conditions, including a different DNA substrate and the less efficient Mg^{2+} activating ions (Supplementary Figure S3A). Moreover, the Y89D mutant and WT PrimPol were similarly stimulated by PolDIP2 (Supplementary Figure S3B), an accessory protein described to be a PrimPol partner (35), and equally efficient to cooperate with Polγ for coupling primer synthesis and processive elongation (Supplementary Figure S3C). The *in vitro* discrepancies between our study and that of Keen *et al.* (21) could be explained by differences in protein expression and purification. In contrast with the results reported (21), the WT and Y89D PrimPol mutant proteins used in our study had very similar CD spectra (Figure 3B), suggesting unaltered overall protein structure of the mutant. This result further supports the hypothesis that the Y89D mutation only has a minor effect on the catalytic activities of PrimPol.

Furthermore, our *in vivo* results show that Y89D is perfectly capable of substituting for endogenous PrimPol in an unchallenged S phase and during the response to UV irradiation or dNTPs attrition. In this case, the *in vivo* discrepancies could be related to the fact that Keen *et al.* (21) reconstituted the loss of endogenous PrimPol in avian DT40 cells with human PrimPol, a heterologous system that may not be suitable to validate the activity of human PrimPol mutations. More importantly, a subsequent genetic study has revealed that Y89D is a common polymorphic PrimPol variant that appears in the control population with similar frequency than in patients with High Myopia (23). This genetic study combined with our functional analysis of the Y89D mutation do not support the conclusions of Zhou *et al.* (20) and Keen *et al.* (21), and the more recent proposal that the Y89D polymorphism could be also associated to PEO (22). Consequently, we suggest that several annotations that the Y89D mutation of human PrimPol is pathogenic and related to High Myopia ought to be reconsidered (i.e. https://www.omim.org/entry/615421; https://www.ncbi.nlm.nih.gov/clinvar/RCV000055646.2/).

CONCLUDING REMARKS

We have identified a conserved motif (WFYY) in the N-terminal domain of human PrimPol, whose flanking amino acids (Trp^{87} and Tyr^{90}) are invariant in other eukaryotic and archaeal PrimPols. On the other hand, Phe^{88} and Trp^{89} residues were conserved only in PrimPols from vertebrates. In agreement with their structural conservation, Trp^{87} and Tyr^{90} were shown to be crucial for the stability of the 3′-incoming nucleotide at human PrimPol active site. Accordingly, W87G and Y90D mutants destroyed PrimPol abilities as a primase and TLS polymerase, and also the capacity to re-start stalled replication forks challenged by UV damage or dNTP deprivation.

Interestingly, the human PrimPol variant F88L, located at the WFYY motif, could substitute for the function of endogenous PrimPol in an unperturbed S-phase, but not when the forks were stalled by UV or HU. As the ability to restart forks resides mainly in the primase activity of PrimPol (3,5,14,15,32,36), these results suggest that the reduced primase activity of the F88L variant is capable of dealing with endogenous fork stalling, but fails to do so when DNA replication is extensively challenged with UV irradiation or dNTP attrition. Finally, human PrimPol mutant Y89D did not significantly affect the PrimPol *in vivo* activities tested, questioning the reported Y89D correlation with High Myopia (20,21) and PEO (22).

DATA AVAILABILITY

'Multiple sequence alignment with hierarchical clustering' F. CORPET, 1988, Nucl. Acids Res., 16 (22), 10881-10890. http://multalin.toulouse.inra.fr/multalin/

SUPPLEMENTARY DATA

Supplementary Data are available at NAR Online.

ACKNOWLEDGEMENTS

This article is dedicated to the memory of Samuel H. Wilson who passed away on 23 April 2021.

FUNDING

BFU2015-65880-P (MINECO) and PGC2018-093576-B.C21 (MCI/AEI/FEDER, UE) to L.B., BFU2016-80402-R (MINECO/FEDER, UE) and PID2019-106707RB-100 (AEI/10.13039/501100011033) to J.M., Kempe JCK 1831 to G.S, Knut och Alice Wallenbergs Foundation KAW 2019.0307, VR-2018-02781, to S.W., and by institutional grants from Fundación Ramón Areces and Banco de Santander to the Centro de Biología Molecular Severo Ochoa; P.A.C. and M.D. were recipients of FPI-predoctoral fellowships from Spanish Ministry of Economy and Competitiveness. Funding for open access charge: Consejo Superior de Investigaciones Científicas.
Conflict of interest statement. None declared.

REFERENCES

1. Frick,D.N. and Richardson,C.C. (2001) DNA primases. *Annu. Rev. Biochem.*, **70**, 39–80.
2. Arezi,B. and Kuchta,R.D. (2000) Eukaryotic DNA primase. *Trends Biochem. Sci.*, **25**, 572–576.
3. Mouron,S., Rodriguez-Acebes,S., Martinez-Jimenez,M.I., Garcia-Gomez,S., Chocron,S., Blanco,L. and Mendez,J. (2013) Repriming of DNA synthesis at stalled replication forks by human PrimPol. *Nat. Struct. Mol. Biol.*, **20**, 1383–1389.
4. Garcia-Gomez,S., Reyes,A., Martinez-Jimenez,M.I., Chocron,S., Mouron,S., Terrados,G., Powell,C., Salido,E., Mendez,J., Holt,I.J. and Blanco,L. (2013) PrimPol, an archaic primase/polymerase operating in human cells. *Mol. Cell*, **52**, 541–553.
5. Torregrosa-Muñumer,R., Forslund,J.M.E., Goffart,S., Pfeiffer,A., Stojkovic,G., Carvalho,G., Al-Furoukh,N., Blanco,L., Wanrooij,S. and Pohjoismaki,J.L.O. (2017) PrimPol is required for replication reinitiation after mtDNA damage. *Proc. Natl. Acad. Sci. U.S.A.*, **114**, 11398–11403.
6. Lipps,G., Rother,S., Hart,C. and Krauss,G. (2003) A novel type of replicative enzyme harbouring ATPase, primase and DNA polymerase activity. *EMBO J.*, **22**, 2516–2525.
7. Sanchez-Berrondo,J., Mesa,P., Ibarra,A., Martinez-Jimenez,M.I., Blanco,L., Mendez,J., Boskovic,J. and Montoya,G. (2012) Molecular architecture of a multifunctional MCM complex. *Nucleic Acids Res.*, **40**, 1366–1380.
8. Bocquier,A.A., Liu,l., Cann,I.K., Komori,K., Kohda,D. and Ishino,Y. (2001) Archaeal primase: bridging the gap between RNA and DNA polymerases. *Curr. Biol.* **11**, 452–456.
9. Keen,B.A., Jozwiakowski,S.K., Bailey,L.J., Bianchi,J. and Doherty,A.J. (2014) Molecular dissection of the domain architecture and catalytic activities of human PrimPol. *Nucleic Acids Res.*, **42**, 5830–5845.
10. Iyer,L.M., Koonin,E.V., Leipe,D.D. and Aravind,L. (2005) Origin and evolution of the archaeo-eukaryotic primase superfamily and related palm-domain proteins: structural insights and new members. *Nucleic Acids Res.*, **33**, 3875–3896.
11. Martinez-Jimenez,M.I., Calvo,P.A., Garcia-Gomez,S., Guerra-Gonzalez,S. and Blanco,L. (2018) The Zn-finger domain of human PrimPol is required to stabilize the initiating nucleotide during DNA priming. *Nucleic Acids Res.*, **46**, 4138–4151.
12. Blanco,L., Calvo,P.A., Diaz-Talavera,A., Carvalho,G., Calero,N., Martínez-Carrón,A., Velázquez-Ruiz,C., Villadangos,S., Guerra,S. and Martínez-Jiménez,M.I. (2019) Mechanism of DNA synthesis by human PrimPol. *Enzymes*, **45**, 289–310.
13. Wan,L., Lou,J., Xia,Y., Su,B., Liu,T., Cui,J., Sun,Y., Lou,H. and Huang,J. (2013) hPrimpol1/CCDC111 is a human DNA primase-polymerase required for the maintenance of genome integrity. *EMBO Rep.*, **14**, 1104–1112.
14. Schiavone,D., Jozwiakowski,S.K., Romanello,M., Guilbaud,G., Guilliam,T.A., Bailey,L.J., Sale,J.E. and Doherty,A.J. (2016) PrimPol is required for replicative tolerance of G quadruplexes in vertebrate cells. *Mol. Cell*, **61**, 161–169.
15. González-Acosta,D., Blanco-Romero,E., Ubieto-Capella,P., Mutreja,K., Míguez,S., Llanos,S., García,F., Muñoz,J., Blanco,L., Lopes,M. and Méndez,J. (2021) PrimPol-mediated repriming facilitates replication traverse of DNA interstrand crosslinks. *EMBO J.*, **15**, e106355.
16. Martinez-Jimenez,M.I., Garcia-Gomez,S., Bebenek,K., Sastre-Moreno,G., Calvo,P.A., Diaz-Talavera,A., Kunkel,T.A. and Blanco,L. (2015) Alternative solutions and new scenarios for translesion DNA synthesis by human PrimPol. *DNA Repair*, **29**, 127–138.
17. Zafar,M.K., Ketkar,A., Lodeiro,M.F., Cameron,C.E. and Eoff,R.L. (2014) Kinetic analysis of human PrimPol DNA polymerase activity reveals a generally error-prone enzyme capable of accurately bypassing 7,8-dihydro-8-oxo-2′-deoxyguanosine. *Biochemistry*, **53**, 6584–6594.
18. Calvo,P.A., Sastre-Moreno,G., Perpiñá,C., Guerra,S., Martínez-Jiménez,M.I. and Blanco,L. (2019) The invariant glutamate of human PrimPol DxE motif is critical for its Mn^{2+}-dependent distinctive activities. *DNA Repair*, **77**, 65–75
19. Rechkoblit,O., Gupta,Y.K., Malik,R., Rajashankar,K.R., Johnson,R.E., Prakash,L., Prakash,S. and Aggarwal,A.K. (2016) Structure and mechanism of human PrimPol, a DNA polymerase with primase activity. *Sci. Adv.*, **2**, e1601317.

20. Zhou,F., Wu,J., Xue,A., Su,Y., Wang,X., Lu,X., Zhou,Z., Qu,J. and Zhou,X. (2013) Exome sequencing reveals CCDC111 mutation associated with high myopia. *Hum. Genet.*, **132**, 913–921.
21. Keen,B.A., Bailey,L.J., Jozwiakowski,S.K. and Doherty,A.J. (2014). Human PrimPol mutation associated with high myopia has a DNA replication defect. *Nucleic Acids Res.*, **43**, 1056–1068.
22. Kasamo,K., Nakamura,M., Daimou,Y. and Sano,A. (2020) A *PRIMPOL* mutation and variants in multiple genes may contribute to phenotypes in a familial case whith chronic progressive external ophtalmoplegia symptoms. *Neurosci. Res.*, **157**, 58–63.
23. Li,J. and Zhang,Q. (2015). PRIMPOL mutation: Functional study does not always reveal the truth. *Invest. Ophtalmol. Vis. Sci.*, **56**, 1181–1182.
24. Boldinova,E.O., Stojkovič,G., Khairullin,R., Wanrooij,S. and Makarova,A.V. (2017) Optimization of the expression, purification and polymerase activity reaction conditions of recombinant human PrimPol. *PLoS One*, **12**, e0184489.
25. Corpet,F. (1988) Multiple sequence alignment with hierarchical clustering. *Nucleic Acids Res.*, **16**, 10881–10890.
26. Cavanaugh,N.A. and Kuchta,R.D. (2009) Initiation of new DNA strands by the herpes simplex virus-1 primase-helicase complex and either herpes DNA polymerase or human DNA polymerase alpha. *J. Biol. Chem.*, **284**, 1523–1532.
27. Stojkovič,G., Makarova,A., Wanrooij,P.H., Forslund,J., Burgers,P.M. and Wanrooij,S. (2016) Oxidative damage stalls the human mitochondrial replisome. *Sci. Rep.*, **6**, 28942.
28. Forslund,J.M.E., Pfeiffer,A., Stojkovič,G., Wanrooij,P.H. and Wanrooij,S. (2018) The presence of rNTPs decreases the speed of mitochondrial DNA replication. *PLoS Genet.*, **14**, e1007315.
29. Díaz-Talavera,A., Calvo,P.A., González-Acosta,D., Díaz,M., Sastre-Moreno,G., Blanco-Franco,L., Guerra,S., Martínez-Jiménez,M.I., Méndez,J. and Blanco,L. (2019) A cancer-associated point mutation disables the steric gate of human. *PrimPol. Sci. Rep.*, **9**, 1121.
30. Kaguni,L.S. (2004) DNA polymerase gamma, the mitochondrial replicase. *Annu. Rev. Biochem.*, **73**, 293–320.
31. Stumpf,J.D. and Copeland,W.C. (2011) Mitochondrial DNA replication and disease: insights from DNA polymerase γ mutations. *Cell Mol. Life Sci.*, **68**, 219–233.
32. Šviković,S., Crisp,A., Tan-Wong,S.M., Guilliam,T.A., Doherty,A.J., Proudfoot,N.J., Guilbaud,G. and Sale,J.E. (2019) R-loop formation during S phase is restricted by PrimPol-mediated repriming. *EMBO J.*, **38**, e99793.
33. Morgado-Palacin,I., Day,A., Murga,M., Lafarga,V., Anton,M.E., Tubbs,A., Chen,H.T., Ergan,A., Anderson,R., Bhandoola,A. *et al.* (2016) Targeting the kinase activity of ATR and ATM exhibits antitumoral activity in mouse models of MLL rearranged AML. *Sci. Signal*, **9**, ra91.
34. Agudo,R., Calvo,P.A., Martinez-Jimenez,M.I. and Blanco,L. (2017) Engineering of human PrimPol into an efficient RNA-dependent-DNA primase/polymerase. *Nucleic Acids Res.*, **45**, 9046–9058.
35. Guilliam,T.A., Bailey,L.J., Brissett,N.C. and Doherty,A.J. (2016) PolDIP2 interacts with human PrimPol and enhances its DNA polymerase activities. *Nucleic Acids Res.*, **44**, 3317–3329.
36. Kobayashi,K., Guilliam,T.A., Tsuda,M., Yamamoto,J., Bailey,L., Iwai,I., Takeda,S., Doherty,A. and Hirota,J.K. (2016) Repriming by PrimPol is critical for DNA replication restart downstream of lesions and chain-terminating nucleosides. *Cell Cycle*, **15**, 1997–2008.